small methods
www.small-methods.com

Optical Binding-Driven Micropatterning and Photosculpting with Silver Nanorods

*M. Carmen Gonzalez-Garcia, Emilio Garcia-Fernandez, Jose L. Hueso, Pedro M. R. Paulo, and Angel Orte**

Controlling the nano- and micropatterning of metal structures is an important requirement for various technological applications in photonics and biosensing. This work presents a method for controllably creating silver micropatterns by laser-induced photosculpting. Photosculpting is driven by plasmonic interactions between pulsed laser radiation and silver nanorods (AgNRs) in aqueous suspension; this process leads to optical binding forces transporting the AgNRs in the surroundings, while electronic thermalization results in photooxidation, melting, and ripening of the AgNRs into well-defined 3D structures. This work call these structures Airy castles due to their structural similarity with a diffraction-limited Airy disk. The photosculpted Airy castles contain emissive Ag nanoclusters, allowing for the visualization and examination of the aggregation process using luminescence microscopy. This work comprehensively examines the factors that define the photosculpting process, namely, the concentration and shape of the AgNRs, as well as the energy, power, and repetition rate of the laser. Finally, this work investigates the potential applications by measuring the metal-enhanced luminescence of a europium-based luminophore using Airy castles.

1. Introduction

Fine control over the preparation of bottom-up nanostructures is a crucial step in current nanotechnology applications. For this, a major advancement was the discovery of the optical trapping effect, by which the interaction of light with micro- and nanostructures resulted in biased diffusion, ultimately leading to actual nanomanipulation of particles on the nanometer scale with a high spatial and temporal resolution with so-called optical tweezers.[1] Nevertheless, research on more finely controlled nanomanipulation has led to other approaches,[2] such as the use of structured illumination[3] or plasmonic nanostructures to enhance the optical trapping resolution.[4] An effect that boosts controlling particles at the nanometer scale is optical binding, which has attracted much attention in the field of nanotechnology in the last few years. Optical binding is contained in the interwoven forces mutually exerted between different scattering particles and leads to self-organized nanostructured arrangements, in which the particles are bound by light–matter interactions without physical contact.[5] According to the mechanism proposed by Huang et al.,[6] nanoparticles (NPs) are initially optically trapped by the laser at a focal point where they align perpendicularly to the polarization of the light beam. The trapped NPs can then efficiently scatter the laser out of the focal volume, leading to the entrapment of other NPs; these NPs can induce multiple scattering events and trap NPs that are farther away.[6] Notably, the light scattered by the trapped particles can travel long distances, even out of the irradiation spaces, leading to optical

M. C. Gonzalez-Garcia[+], E. Garcia-Fernandez, A. Orte
Nanoscopy-UGR Laboratory
Departamento de Fisicoquímica
University of Granada
Campus Cartuja, 18071 Granada, Spain
E-mail: angelort@ugr.es

The ORCID identification number(s) for the author(s) of this article can be found under https://doi.org/10.1002/smtd.202300076

[+]Present address: nanoFRET.com, Laboratoire COBRA (Chimie Organique, Bioorganique, Réactivite et Analyse), UMR 6014, CNRS, Université de Rouen Normandie, Mont-Saint-Aignan Cedex, INSA, 76821 Rouen, France

DOI: 10.1002/smtd.202300076

J. L. Hueso
Instituto de Nanociencia y Materiales de Aragón (INMA)
CSIC-Universidad de Zaragoza
Campus Rio Ebro, 50018 Zaragoza, Spain

J. L. Hueso
Department of Chemical and Environmental Engineering
University of Zaragoza
Campus Rio Ebro, 50018 Zaragoza, Spain

J. L. Hueso
Networking Res. Center in Biomaterials
Bioengineering and Nanomedicine (CIBER-BBN)
Instituto de Salud Carlos III
28029 Madrid, Spain

P. M. R. Paulo
Centro de Química Estrutural
Institute of Molecular Sciences
Instituto Superior Técnico
Universidade de Lisboa
1049-001 Lisboa, Portugal

binding in the nonirradiated areas. This effect has been used to achieve controlled nanoarrangements of silver[7] and gold NPs.[8] or polystyrene particles.[9] Working at the single particle level leads to dynamic but well-ordered structures. However, stable nanoarrangements with metal NPs need to overcome the increase in the kinetic energy of the particles and, therefore, a greater Brownian motion caused by a heightened temperature due to the strong absorption of light.[4,10] This enhanced mobility of the NPs, together with the rest of the forces exerted on them, produces a swarming effect of the NPs around the focal point when the NP concentration is relatively high.[6] In the swarming effect, light scattering plays a critical role, as demonstrated by the dependency of the optical binding on the polarization of the irradiation beam.[5,6,8,9]

However, optical binding nanomanipulation is usually performed in an off-resonance fashion to ensure that the metal plasmons of the metallic NPs are not involved in the process. Usually, plasmonic interactions between high-fluence laser radiation and metal NPs result in several effects on the shape and size of the NPs, especially when large photon densities from pulsed sources are employed. The effects of pulsed lasers on Au nanosized particles have been extensively studied, involving reshaping, thinning, or fracturing.[11] Such effects were reported by Link et al. for colloidal Au nanorods (NRs)[11] but were successively exploited to controllably reshape Au NPs into highly monodispersed nanorods[12] or submicrometer particles.[11] Similar reshaping effects were also reported for Ag NPs but required a rigid matrix achieved using glass-embedded nanocomposites.[13]

In this work, we describe a method for photosculpting 3D Ag structures by picosecond pulsed, UV–visible laser light interacting with AgNRs. AgNRs exhibit strong plasmonic light-matter interactions since the rod symmetry allows for two different localized surface plasmon resonances (LSPRs) (transversal and longitudinal).[14] Such LSPR can be used for multiple sensing and biological applications, such as surface-enhanced Raman spectroscopy (SERS) imaging.[15] In our study, light-AgNR interactions drive optical binding and swarming effects, followed by photooxidation, reshaping, melting, and ripening of the AgNRs. This method results in very stable Ag nanostructures photosculpted on glass slides, which can be controllably generated in micropatterns, with potential applications in nanophotonics. Herein, we also demonstrate how these structures can be used as plasmonic centers for metal-enhanced luminescence (MEF) of a selected luminophore.

2. Results and Discussion

2.1. Swarming and Photosculpting with AgNRs

Since the photon momentum is inversely proportional to its wavelength, we used a pulsed, 375 nm laser diode directed through an objective lens of a confocal microscope to promote the swarming of plasmonic AgNRs, as well as directly interacting with the LSPR of the AgNRs (**Figure 1**). For these experiments, we used AgNRs exhibiting an average longitudinal:transversal ratio of 2.2 ± 0.3, resulting in two surface plasmon absorption transitions, centered at 415 and 600 nm for the transversal and longitudinal LSPRs, respectively (Figure S1, Supporting Information). These AgNRs were synthesized and purified in our lab, as described in the Experimental Section and Figures S1 and S2, Supporting Information).

The optical trapping and swarming effect caused by the 375 nm pulsed laser was effectively confirmed by the light scattering patterns detected by the CCD camera showing the back-reflection of the laser light (Figure S3 and Video S1, Supporting Information). Importantly, focusing and trapping AgNRs near the glass slide surface led to a very interesting phenomenon. As discussed below, the interaction of the pulsed laser light with the AgNR plasmons caused an increase in local temperature, photooxidation, partial melting, and ripening so that AgNRs coalesced on a controlled photosculpting of metallic silver in the irradiated spots in less than 1 min. This effect could also be directly observed by the temporal increase in back-scattered light (Figure S4 and Video S2, Supporting Information). By using this process, we were able to controllably design micropatterns of photosculpted silver structures (Figure 1B). Scanning electron microscopy (SEM) with energy-dispersive X-ray spectroscopy (EDX) analysis confirmed that the photosculpted spots contained silver (Figure S5, Supporting Information). Such photosculpted aggregates were subsequently imaged using confocal microscopy. The same 375 nm laser was used for imaging (at low power), and the fast raster scan of the images (0.6 ms dwell time) did not alter the photosculpted structures. The sculpted Ag micropatterns were stable and remained immobile on the glass surface upon washing with Milli-Q water or ethanol (Figure S6, Supporting Information).

The photosculpted structures were imaged using a 630/60 nm bandpass filter. This band did not correspond to the scattered light (Rayleigh or Raman) or optical harmonics of the incident laser. Hence, the detected light came from luminescent species within the microstructure. To explain the nature of the detected radiation, we used spectral imaging combined with confocal imaging[16] to extract the wavelength distribution of this light. Figure 1C shows the photoluminescence (PL) emission spectra collected at the photosculpted structures. The PL emission spectra exhibited features with a band centered at 510 nm and a broad band in the 575–675 nm range. We confirmed the spectral distribution of the PL emission and the detected light in the microscope by simultaneously using four detectors in the microscope, using bandpass filters of 450/40, 500/40, 550/40, and 630/60 nm. The signals were spectrally corrected according to the detectors' performance and the optical elements, and the results were compared with the obtained spectrum (Figure 1C), showing excellent agreement between the two techniques and confirming that the 630/60 filter was optimal to image the photosculpted structures. Importantly, the 575–675 nm PL band correlates with emissive Ag nanoclusters of the type Ag_x^{+l} (with $x = 2, 3, \ldots$ and $l = 1, 2, \ldots$), which are known to emit PL between 550 and 700 nm, depending on the size, the environment,[17] or the excitation wavelength,[18] and exhibit dual-band emission properties.[19] The formation of Ag nanoclusters upon irradiation of AgNPs with a pulsed laser has been previously reported in studies of NP reshaping[13b] and within micrometer-sized Ag wires.[20] Indeed, the energy and fluence of our tightly focused laser are sufficient to generate photooxidation of Ag into ions through the ejection of photothermal electrons.[13a,21] Several cycles of Ag^+ ejection and recapturing electrons lead to shape alteration in Ag NPs,[13a] along with the formation of emissive Ag_x^{+l} nanoclusters.[13b,21] Moreover,

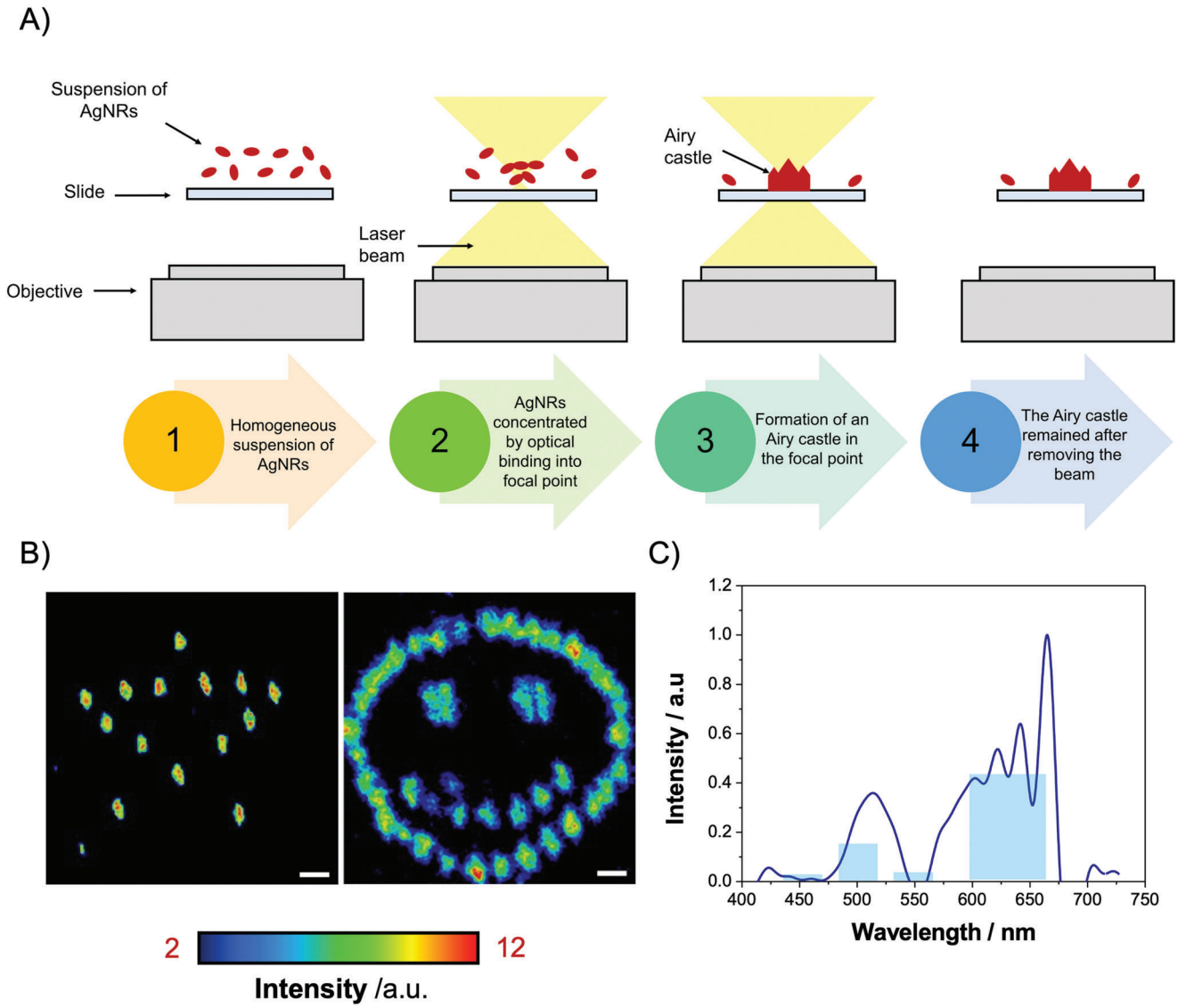

Figure 1. A) Scheme of the swarming and trapping effect of the silver nanorods (AgNRs) (localized surface plasmon resonance (LSPR) = 600 nm) by a 375 nm laser beam through an objective lens of a confocal microscope and the subsequent photosculpting of Airy castles. B) Confocal microscopy intensity images obtained after irradiating micropatterned spots (375 nm, 20 MHz repetition rate, 9.4 μW, 1 min irradiation) with a suspension of AgNRs (LSPR = 600 nm, 60×10^{-3} M). Scale bars represent 1 μm. C) Normalized emission spectrum of Airy castles ($\lambda_{exc} = 375$ nm) obtained on a spectrograph coupled to a confocal microscope, with 20 accumulations over 10 s (blue line), and integrated normalized emission intensity recorded by each detector of the confocal microscope (with filters 450/40, 500/40, 550/40, and 630/30) (blue bars).

the band at 510 nm supports the presence of photo-oxidized Ag^+ ions known to emit PL at this spectral region due to Laporte forbidden transitions.[13b] In fact, the presence of small nanoclusters upon irradiation of NPs has not only been detected through their luminescent properties but also imaged using transmission electron microscopy (TEM), usually found as a halo of very small NPs surrounding the irradiated specimen for both Ag[13] and Au NPs.[11d,e]

We then investigated the laser-induced photosculpting phenomenon in detail to optimize the conditions leading to controllable micropatterning. For this, we focused on the real-time kinetics of the formation of Ag nanoclusters during irradiation through their PL emission. We fitted the kinetic traces to an exponential growth equation (Equation 1 in the Experimental section). The concentration of the AgNRs was controlled from 15×10^{-12} M to 120×10^{-12} M particles (see Supporting Information for details on the method used to determine the concentration of AgNRs). Additionally, we studied the effect of silanizing at the glass surface (see the Experimental section and Figure S6A, Supporting Information) and found that although bare slides provided faster kinetics, the photosculpting was much more controllable on the silanized surfaces (Figure S6A, Supporting Information). We then studied the dependency of the photosculpting on the concentration of the AgNRs and the repetition rate of the irradiation laser. The laser repetition rate was changed from 2.5 to 40 MHz, leading to different average laser power values (3.1 μW

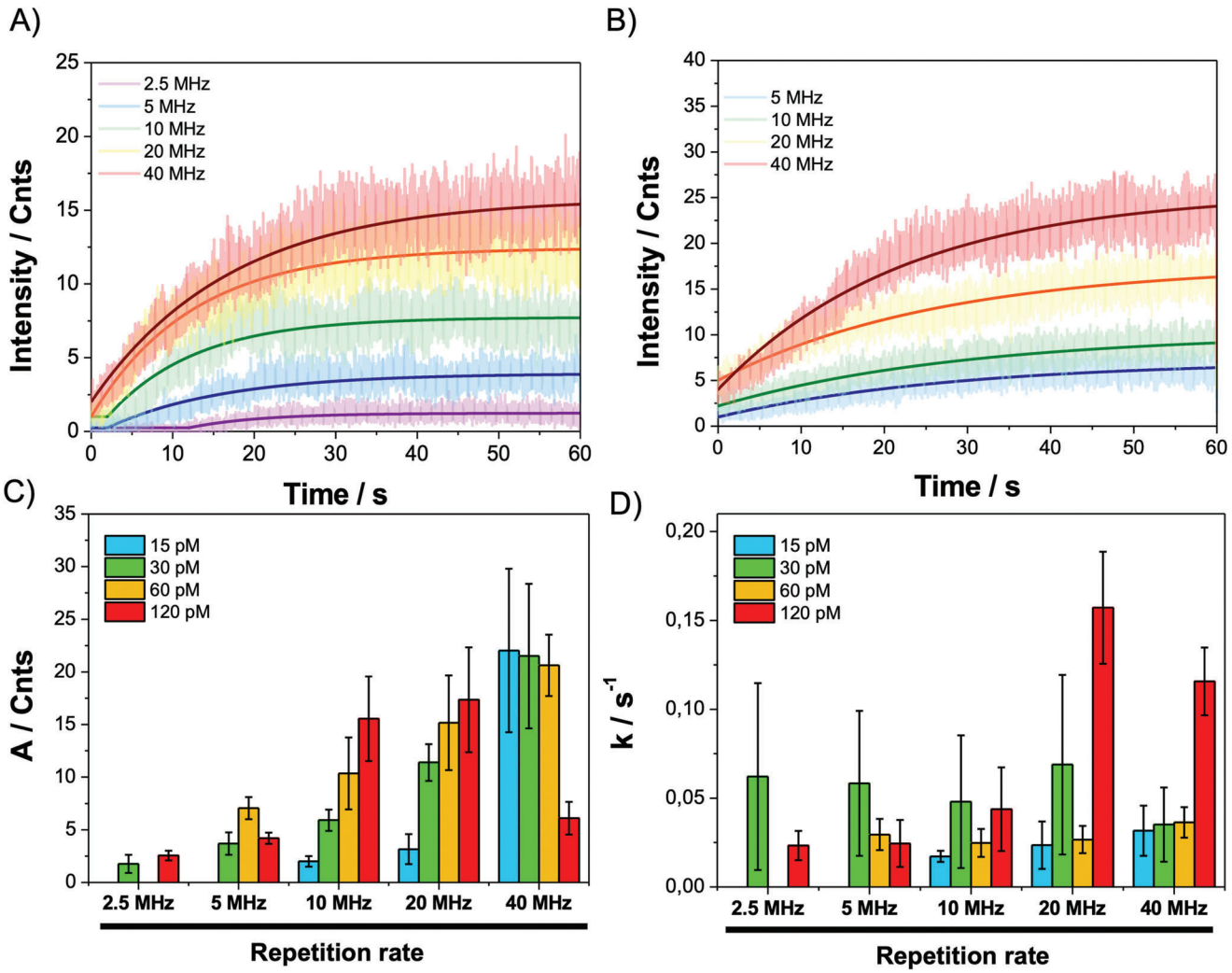

Figure 2. Intensity time traces for photosculpting events of the silver nanorods (AgNRs) (localized surface plasmon resonance (LSPR) = 600 nm) at A) 30×10^{-12} M and B) 60×10^{-12} M by a pulsed, 375 nm laser at different repetition rates. Dark solid lines represent the fitting to the exponential rise function (Equation 1). C) Average amplitude, *A*, and D) rate constant, *k*, values obtained from the fittings of 6–12 independent photosculpting events.

@ 2.5 MHz; 6.4 μW @ 5 MHz; 13.7 μW @ 10 MHz; 28.2 μW @ 20 MHz; 62 μW @ 40 MHz); since we only modified the repetition rate without changing any other parameter of the laser driver or the optical path, the punctual power of each pulse remained constant, and the overall power only varied due to a larger or lower number of pulses per second (Figure S7, Supporting Information). **Figure 2**A and Figure S8 (Supporting Information) show representative photosculpting kinetic traces under different experimental conditions, whereas Figure 2B shows the corresponding average *A* and *k* values obtained from the fittings of 6–12 repetitions to equation 1. We observed a clear increase in both the amplitude and the rate constant with increasing concentration of the AgNRs. Moreover, an increase in frequency led to an increase in the amplitude of the PL emission (Figure S9, Supporting Information), although it did not show a simultaneous increase in the photosculpting rate. At least 10 MHz was required to trigger photosculpting with 15×10^{-12} M AgNRs, but at 10 and 20 MHz, the amplitude was not large. At higher concentrations of AgNRs, the amplitude grew steadily with increasing frequency. The rate values also showed a certain dependency on the AgNR concentration; as expected, the largest rates were found at 120×10^{-12} M due to more particles being attracted to the swarm. This factor led to the consideration of a second-order kinetics model for the photosculpting process with respect to AgNRs. This was consistent with the fact that several AgNRs needed to be bound together through the optical binding force, encountered and, finally, coalesced for effective photosculpting. However, the results at low frequency and low AgNR concentration indicated that a certain threshold value was required for the process to occur. Figure S10 and Video S3 (Supporting Information) illustrate the effect of the photoirradiation time on the formed deposited micropatterns. As expected, longer irradiation times resulted in larger structures as more AgNRs traveled into the photosculpted structure.

We used atomic force microscopy (AFM) to closely examine the photosculpted micropatterns. Photosculpting with the AgNRs was performed, following the same procedure, on a silanized glass slide surface using a reference grid to easily

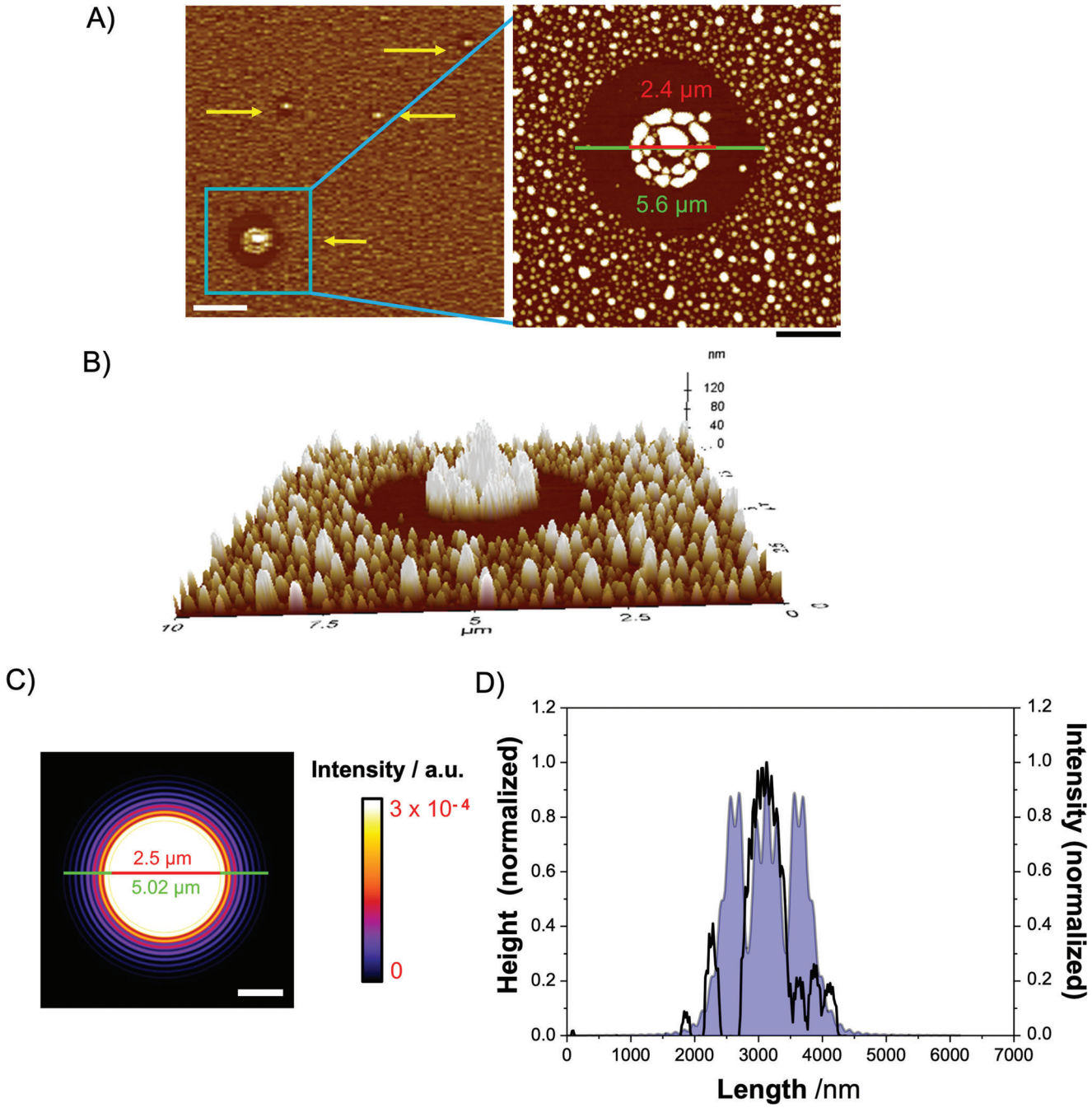

Figure 3. A) Representative noncontact atomic force microscopy (AFM) imaging of a photosculpted structure with the silver nanorods (AgNRs) (localized surface plasmon resonance (LSPR) = 600 nm) deposited on a silanized glass slide and irradiated for 1 min at the points marked with arrows with a pulsed, 375 nm laser (28.2 µW at 20 MHz). Scale bar represents 5 µm in the left panel and 2 µm in the right panel. B) 3D reconstruction of the magnified section marked with a square in panel (A) showing the arrangement of a representative Airy castle. C) Simulation of an Airy disk from a 375 nm laser being focused through a 1.4 NA objective at 1 µm above the interfacial surface. D) Comparison of the height trace extracted from the line represented in the AFM image (black line) and the line in the simulated Airy disk (blue, shaded line).

locate the irradiated regions once the slide was moved to the AFM instrument. Noncontact AFM images clearly showed that the surface was covered with NPs of different sizes, but at those irradiated points, photosculpting was clearly identified by a marked accumulation of nanostructures surrounded by a blank halo (**Figure 3**). This profile was clearly indicative of photosculpting being triggered by a swarming effect due to optical binding. Focusing on the largest aggregates (Figure 3B), the resemblance of the formed tower-shaped structures with an Airy disk, a pattern formed by a laser beam being focused through a microscope objective, was remarkable (Figure 3C,D); thus, we coined the term "Airy castles" to refer to the three-dimensional

structures achieved through this selective photosculpting. The different sizes achieved depended on the effective focusing of the laser at the glass surface or a few micrometers above the surface. The Airy disk profile follows the formulation of the Fraunhofer diffraction pattern for a circular aperture;[22] to compare the formed structures with the Airy disk, we simulated the Airy disk pattern produced by a 375 nm laser focused through a 1.4 NA objective at 1 μm above the glass surface (Figure 3C,D) using a dedicated ImageJ plugin.[24] For the simulation, we employed a refractive index of 1.5, corresponding to the immersion oil, 1.4 of numerical aperture, 375 nm for the wavelength, 10 nm for XY pixel size and 250 nm for Z pixel size. The photosculpted area in the Airy castle correlated perfectly with the high-intensity region of the Airy disk, whereas the blank halo in the Airy castle correlated with the steep decrease in intensity of the outer section of the Airy disk. Moreover, this blank region was clearly related to the fact that optical binding could be extended out of irradiated regions through the mutual scattering of particles.[6,8,9] Considering that slight differences in the focus depth may arise during the photosculpting process, we also performed simulations of the Airy disks at different depths of the focal point (Figure S11, Supporting Information). The kinetic traces in Figure 2 clearly demonstrate that photosculpted aggregates were slowly formed through coalescence of several AgNRs. This aggregation led to increased scattering features, hence resulting in optically binding and trapping more AgNRs outside the irradiated area, transporting them into the Airy castle and clearing the nearby area. The effect was saturated, as shown in the kinetic traces, at distances where the optical binding force was not sufficient to attract more AgNRs. Additionally, the use of plasmonic AgNRs could enhance the optical trapping effect.[4] Therefore, the arrangement of the Airy castles clearly demonstrated that photosculpting was triggered by optical trapping of the AgNRs into the high intensity, focused region of the laser, and completed by the optical binding forces outside irradiated areas.

We further explored and optimized other experimental aspects of the photosculpting process, starting with the effects of the AgNR aspect ratio and the wavelength of the LSPR. Along with the AgNRs with LSPR at 600 nm, we tested the AgNRs with longitudinal LSPRs at 470 and 820 nm (aspect ratio values of 2.12 and 4, respectively), as well as spherical AgNPs with a diameter of 8.6 ± 2.6 nm. Photosculpting was feasible with pulsed, 375 nm excitation for all the employed particles (Figures S12 and S13, Supporting Information), although much slower kinetics were found for AgNPs, likely due to their smaller size and higher thermal stability compared to AgNRs,[24] which highlights the importance of using AgNRs in the method (see Supporting Information). Additionally, we tested whether pulsed laser sources of longer wavelengths were capable of selectively promoting photosculpting of the AgNRs (Figure S14, Supporting Information). The tested AgNRs and AgNPs share a plasmon resonance centered at 400 nm, although AgNRs also exhibit an additional longitudinal plasmon resonance at a different wavelength. The 375 nm laser overlaps with the 400 nm plasmon resonance of these NPs, while the 470 and 635 nm lasers do not. The 635 nm laser was not able to produce the aggregation of the AgNRs despite the overlap with the longitudinal LSPR at 600 nm (Figure S14, Supporting Information); this result was probably due to smaller optical trapping forces of the lower energy photons, diminishing the efficiency of the photosculpting dynamics.

All our results can thus be rationalized considering a first step of NP swarming and subsequent ripening into the photosculpted structures. Indeed, we confirmed that optical trapping had an important role as a trigger event for photosculpting and that optical trapping was enhanced when the irradiation wavelength overlapped with the plasmonic bands of the NPs. Then, as aggregates were formed, more scattered light was generated (Figure S4, Supporting Information), triggering the optical binding forces that attracted additional AgNRs into swarms and cleared surrounding areas. Similar swarming and deposition of Au NPs has been reported in studies by Huang et al.[6] and Kudo et al.[25] These authors observed that Au NPs were deposited in different patterns depending on the electric field produced by the laser's Airy disk. Likewise, optical trapping of AgNPs could be achieved by using a >1000 nm NIR laser far from the LSPR absorption of the particles.[10] Nevertheless, these studies reported the accumulation of individual NPs that did not coalesce with each other. In our case, the interaction of photons with the plasmonic absorption generated excited electrons, whose energy excess could be rapidly transferred to the lattice by electron–phonon interactions, thermalized by increasing the temperature[26] and causing emission of electrons,[27] oxidation, and ejection of Ag^+ ions,[13] which in turn gave rise to emissive Ag_x^{+l} nanoclusters.[13] Photosculpting of Airy castles was undoubtedly a result of AgNR melting and ripening, in contrast to other effects found in the literature, such as reshaping,[11-13] thinning,[11] or fragmentation.[11,13] The intermediate step of metal melting has been proposed as crucial in the reshaping of metal NPs, especially involving plasmonic light–matter interactions,[11] and has been used, for instance, to yield submicron-sized Au NPs through particle ripening and growth.[11,28] In fact, the Au NP growth reported by Tsuji et al. shares common features with our photosculpted Airy castles. However, our method exhibits several unique characteristics. In previous works, small nanoclusters were usually expelled out of the particle due to Coulombic repulsion between highly charged particles,[11,13,27] whereas Airy castles maintained luminescent properties since the nanoclusters remained stable within the 3D structure.[20] Another unique feature was that we could perform this method with NPs in aqueous suspension, whereas in the past, Ag nanostructure reshaping was performed in glass-embedded nanocomposites since they required a rigid matrix.[13,21] Moreover, the photosculpted micropatterns even resisted harsh washings so that interfacial Ag-glass interactions were strong, possibly initiated by incorporation of ejected photoelectrons into the glass conduction band.[13]

Controlled photosculpting with AgNRs is an alternative to two-photon absorption laser-induced photoreduction and subsequent deposition in controlled silver micropatterns. This methodology makes use of fs-pulsed lasers and multiphoton excitation of a photosensitizer or photoreducing agent capable of absorbing two photons and subsequently donating electrons to Ag^+ ions, starting the nucleation of Ag NPs that are subsequently deposited, even yielding finely organized motifs.[30] Nevertheless, our methodology has differential features, such as i) instead of using an expensive fs-pulsed laser for multiphoton absorption, we can use a much more affordable ns-pulsed laser; ii) we do not require adding a photosensitizer that in the last terms defines

the size and homogeneity of the photodeposited structures,[30b] so that side-products from an oxidation–reduction reaction are not generated; iii) whereas photoreduction requires large concentrations of Ag^+ ions, usually in the range 0.01–1 M,[30a,c] we work with concentrations of AgNRs in pM levels; and iv) the photosculpting process can be monitored in real time by the formation of luminescent Ag nanoclusters.

The fact that our photosculpting methodology starts upon clusterization of preformed AgNRs would make it directly related to other methods that use preformed NPs for deposition and patterning. For instance, such clusterization has been reported to be mediated by thiol-induced aggregation,[30] salting-out,[31] or photoinduced effects.[32] However, all such methodologies usually lead to dendritic-fractal aggregates, whereas in our case, photosculpting using particles in suspension was controlled by the laser focus and was possible due to optical trapping and optical binding as the driving force for aggregation. This was confirmed by irradiating a suspension of AgNPs focusing the laser inside the aqueous medium instead of at the glass–water interface. This experiment showed clear growth in the AgNP size by melting and ripening, giving rise to an approximate 10-fold increase in particle diameter (Figure S13D, Supporting Information).

In fact, photosculpting with AgNRs yields similar structures to those achieved by plasma-induced oxidation of silver to silver oxide and subsequent removal of the oxide,[33] micropatterns by reducing electron beam lithography,[34] nanoimprint and electrodeposition techniques,[35] or laser-induced ablation, transfer, and deposition,[36] but, in our case, with a much simpler and straightforward approach.

The fact that controllable Airy castle structures can be stably deposited and the pointed tip of the Airy castles pave the way for using plasmonic interactions in micrometer-sized biosensing platforms containing arrays of photosculpted aggregates. As an example, in the next section, we explored the ability of arrayed Airy castles as platforms to foster enhancement of luminescence emission of nearby fluorophores by MEF.

2.2. Plasmonic Interaction of Airy Castles with Luminophores for Metal-Enhanced Fluorescence Detection

The phenomenon of MEF responds to the enhanced electric field on the surface of plasmonic particles. The enhancement is particularly intense in NPs containing sharp tips.[38] The intense electric field at the plasmonic surfaces may result in faster re-excitation cycles for luminophores that lie within 1–10 nm from the plasmonic surfaces, and thus, they undergo an increase in PL emission. Although this phenomenon is not easily controlled due to the required fine control of the position of the luminophore with respect to the plasmonic particle, MEF has been successfully used in the development of biosensors of different types. Recent reviews are available regarding the use of MEF for improved biosensing technologies.[39]

To test the potential of the photosculpted arrays of Airy castles to be used as sensing platforms, involving high sensitivity due to MEF, we performed simulations of the optical response of a modelled Airy castle (see Supporting Information for computational details). Our results confirmed that the Airy castle entails a highly scattering microstructure with broad spectral response (Figure S15, Supporting Information). This may yield MEF for a variety of different dyes. Specifically, we combined Airy castles with a luminophore based on a cryptate of a lanthanide cation such as {2,2',2'',2'''-{4'-{[(4,6-dichloro-1,3,5-triazin-2-yl)amino]biphenyl-4-yl}-2,2':6',2''-terpyridine-6,6''-diyl}bis(methylenenitrilo)}tetrakis(acetato)} europium(III) (DTBTA-Eu(III)).[39] DTBTA-Eu(III) exhibits the main features of emissive lanthanide ions, very narrow PL emission bands and a PL lifetime in the range of ms (**Figure 4**A), which are especially interesting in time-gated imaging analysis.[40] Given the spectral features of DTBTA-Eu(III), we simulated the enhancement factors for the electromagnetic field of 375 and 616 nm radiation in the surroundings of the Airy castle (Figure S16, Supporting Information) and found several hot-spots where MEF could be achieved.

Hence, we experimentally challenged this concept by adding initially a solution of DTBTA-Eu(III) (100×10^{-9} M) onto a preformed pattern of AgNR Airy castles. An F-shaped pattern of Airy castles was obtained as described in the previous section, with a 30×10^{-12} M dilution of the synthesized AgNRs (LSPR = 600 nm). Before the addition of the DTBTA-Eu(III) solution, the slide was washed twice with Milli-Q water and absolute ethanol to remove the excess AgNRs and unstable aggregates. Figure 4 shows that a 20-fold increase in DTBTA-Eu(III) emission intensity was obtained at the points where the AgNRs Airy castles were located. The enhancement of the emission of DTBTA-Eu(III) could be caused by plasmonic effects in the surface of the Airy castles where the dye interacted via adsorption. To confirm the involvement of the MEF, we focused on the effect on the PL lifetime of the dye, which is known to decrease upon MEF-driven emission.[41] Hence, we performed PL lifetime imaging (PLIM) of the emission of DTBTA-Eu(III) interacting with the Airy castles. In these experiments, we carried out the photosculpting of Airy castles with AgNRs (LSPR = 600 nm) in the presence of 600×10^{-9} M DTBTA-Eu(III) but collected the images in PLIM mode. This involves using a 62.5 µs train of pulses, followed by a 5 ms detection time window. Such long imaging times required working at low laser power to prevent further photodeposition, warping the preformed Airy castles. As expected, DTBTA-Eu(III) showed a brighter PL emission in the presence of AgNR Airy castles. The analysis of the PLIM images yielded two PL lifetime components: a long τ of 520 ± 40 µs and a short τ of 2.5 ± 0.7 µs. When analyzing the average lifetime, $<\tau>$, and the amplitude ratio (Figure 4D), one can clearly identify lower $<\tau>$ values, in the range of 35–75 µs, in the Airy castles, correlated with a clear larger abundance of the short τ lifetime, indicating that DTBTA-Eu(III) was quenched in the regions with enhanced emission intensity. Although we cannot discard the accumulation of DTBTA-Eu(III) at the Airy castles due to adsorption, the associated quenching is consistent with an MEF mechanism.[42]

With the aim of controlling the distance between the plasmonic structures of the Airy castles and the studied luminophore, we modified the dye by covalently adding polyethyleneglycol (PEG) chains of different lengths ending on a thiol group, –SH (Figure S17, Supporting Information). In particular, we added either PEG_{200}, PEG_{400}, or PEG_{600} chains to DTBTA-Eu(III) to increase the length of the linker. Thiol groups served as covalent interacting centers of the modified dye with metallic surfaces. In these experiments, we irradiated samples

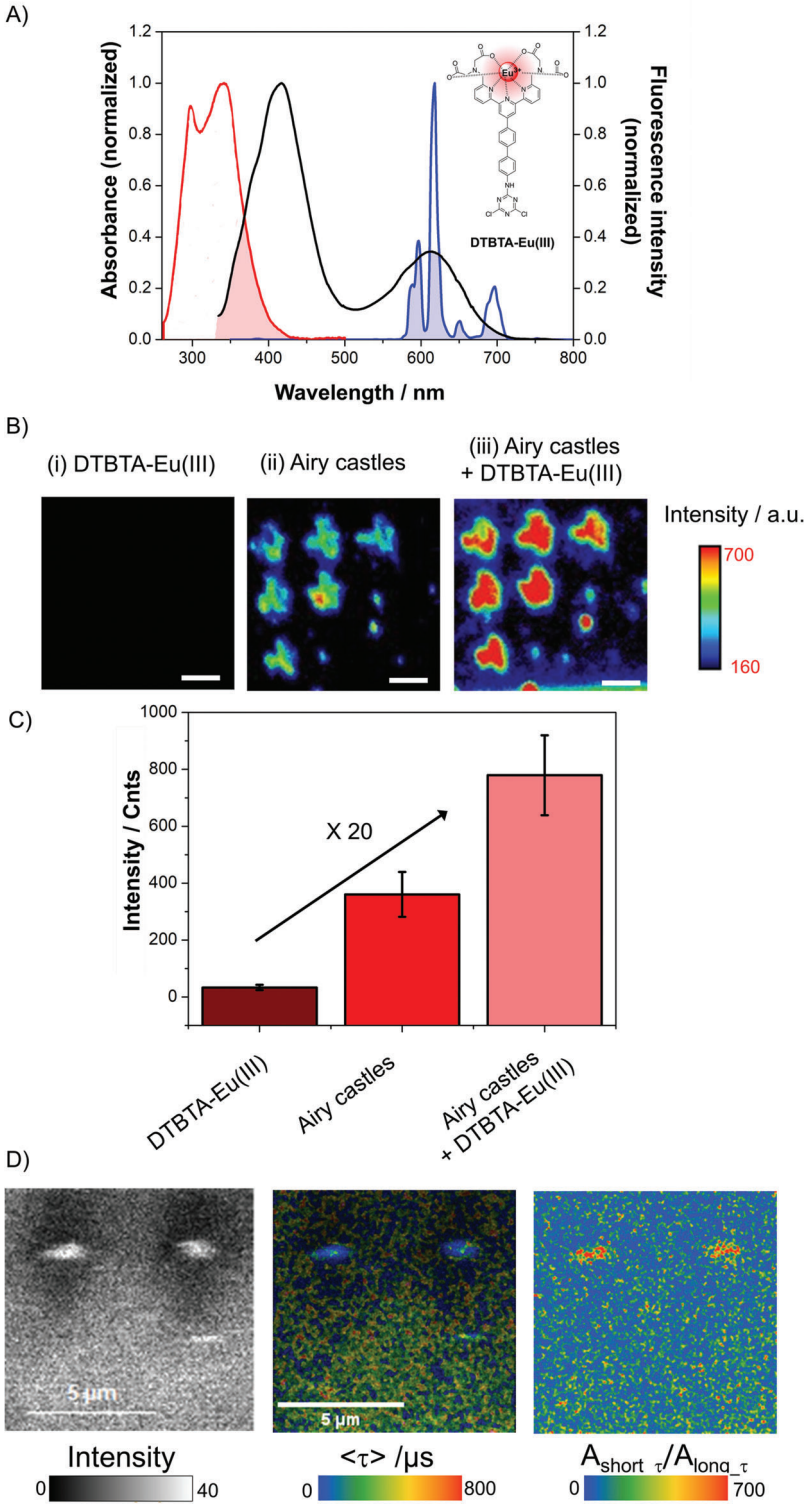

Figure 4. A) Absorption spectra of the silver nanorods (AgNRs) with localized surface plasmon resonance (LSPR) = 600 nm (black) and DTBTA-Eu(III) (red) and emission spectra of DTBTA-Eu(III) (blue). Shaded areas indicate overlapping spectral regions. B) Luminescence confocal microscopy images of (i) 100×10^{-9} M DTBTA-Eu(III) on a silanized coverglass as a control, (ii) an F-shaped pattern of Airy castles of 30×10^{-12} M AgNRs (LSPR = 600 nm) (28.2 µW, 20 MHz), and (iii) the same region as in (ii) after washing the slide twice with water and absolute ethanol and adding 100×10^{-9} M DTBTA-Eu(III). Scale bars represent 2 µm. C) Average intensity at the regions of interest (aggregate spots) from 100×10^{-9} M DTBTA-Eu(III) at the glass surface, AgNR Airy castles, and AgNR Airy castles in the presence of 100×10^{-9} M DTBTA-Eu(III). D) Photoluminescence lifetime imaging (PLIM) confocal microscopy images of Airy castles preformed with 30×10^{-12} M AgNRs (LSPR = 600 nm) after washing the slide and adding 600×10^{-9} M DTBTA-Eu(III). The intensity, average lifetime $<\tau>$, and ratio of amplitudes $A_{short\_\tau}/A_{long\_\tau}$ images are shown. Scale bars represent 5 µm.

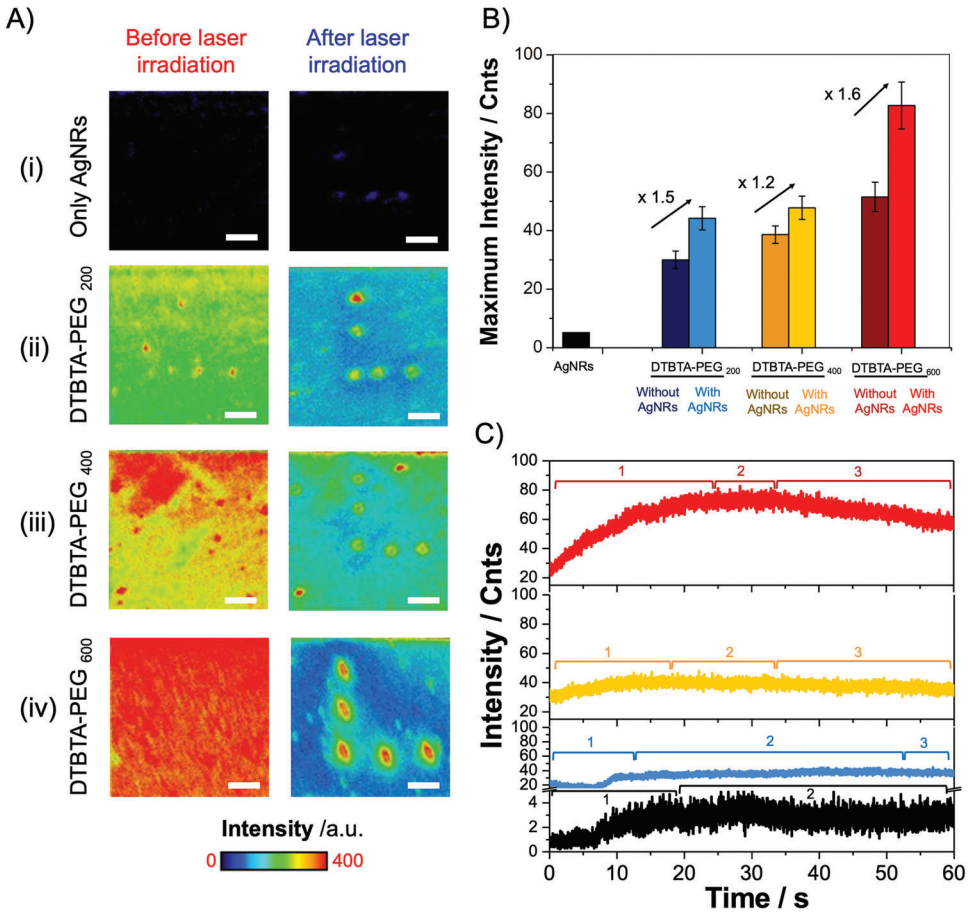

Figure 5. A) Luminescence confocal microscopy images of the silver nanorods (AgNRs) (localized surface plasmon resonance (LSPR) = 600 nm) (i) and with the addition of 10×10^{-6} M of DTBTA-PEG_{200} (ii), DTBTA-PEG_{400} (iii), or DTBTA-PEG_{600} (iv), before and after irradiation in an L-shaped pattern of five Airy castles with the pulsed, 375 nm laser (28.2 μW at 20 MHz) for 1 min. Scale bars represent 2 μm. B) Maximum values of the intensity time traces of DTBTA-PEG_{200}, DTBTA-PEG_{400}, or DTBTA-PEG_{600} in the presence or absence of AgNRs. C) Representative intensity time trace for the photoirradiated spots of the AgNRs alone (black) and the AgNRs in the presence of DTBTA-PEG_{200} (blue), DTBTA-PEG_{400} (yellow), or DTBTA-PEG_{600} (red).

containing both PEGylated-DTBTA-Eu(III) and AgNRs. Before photosculpting, part of the dye was adsorbed onto the glass surface, leading to an emissive background signal. Then, we irradiated an L-shaped pattern of points with the pulsed, 375 nm laser (28.2 μW at 20 MHz) for 1 min at each point; these were the conditions used to promote the photosculpting of Airy castles. Subsequent imaging showed accumulation of emission of the dye at the Airy castles (**Figure 5**A), with mild enhancement factors of approximately 1.5 (Figure 5B). We also compared the kinetics of the photosculpting process (Figure 5C), leading to interesting results. The amplitudes of the overall intensity traces were much larger in the experiments with PEGylated-DTBTA-Eu(III) than with only the AgNRs, indicating that the dye was indeed interacting through the thiol group with the NPs while the aggregates were being formed. Additionally, after the initial growth phase (marked as 1 in the time traces of Figure 5C) and a stabilization phase (marked as 2), a decrease in the emission intensity of the dye was detected (marked as phase 3) due to photobleaching caused by the irradiation laser. The latter was demonstrated by irradiating adsorbed dye on the glass slide under the same conditions but in the absence of the AgNRs (Figure S18, Supporting Information).

3. Conclusion

We have demonstrated selective melting of different AgNRs in suspension and subsequent photosculpting into well-defined, 3D, aggregated structures, driven by a swarming effect caused by a pulsed, 375 nm laser. We have named those structures Airy castles due to their resemblance to the interference pattern of an Airy disk. Studying the kinetics of this process showed the effect of the AgNR concentration, laser power and energy. The swarming effect of AgNRs was caused by optical trapping forces, but the effective formation of the Airy castles also required a certain concentration of particles and an irradiation wavelength that matched the short wavelength plasmon resonance of the particles. The interaction of tightly focused, pulsed radiation with the transversal LSPR of the AgNRs led to optical trapping and binding, photooxidation, and thermionic emission of electrons, finally resulting in melting and ripening into the photosculpted Airy castles, which were stable with time and resistant to harsh washes. The Airy castles distinctively maintained PL emission owing to the surface presence of Ag nanoclusters formed during the photosculpting process. We also confirmed the enhancement of luminescence caused by MEF using arrayed patterns of Airy castles as the

centers for localizing a long-luminescence lifetime dye, europium cryptate DTBTA-Eu(III). The methodology presented herein provides an interesting alternative to two-photon absorption photoreduction, nanoimprint, and electrodeposition techniques or reducing electron beam lithography. The main advantage of our proposed methodology is that the micrometer-sized array can be freshly prepared on-site using the same microscope that would be subsequently used in a biosensing approach; once the array is preformed, it can be stored and used when needed due to its high stability. These concepts will promote the further development of microarray-based biosensing applications.

4. Experimental Section

Materials: For AgNR synthesis and purification, Milli-Q water (≤18.2 MΩ.cm), ethylene glycol (EG) (anhydrous, 99.8%), $AgCOOF_3$ (98%), polyvinylpyrrolidone (PVP, MW = 1.3×10^6 g mol^{-1}), tannic acid, HCl (37%), $AgNO_3$ (>99%), sodium citrate dihydrate and $NaBH_4$, were used. All reagents were purchased from Sigma–Aldrich (Germany). The AgNRs were synthesized following the protocol described by Patarrollo et al.[43] with few modifications; they were purified by centrifugation in a glycerol gradient (see Supporting Information for full details).

DTBTA-Eu(III) was synthesized from ATBTA-Eu(III) (purchased from Tokyo Chemical Industry Co. Ltd., Japan) following the procedure described by Nishioka et al.[40] For PEGylation of DTBTA-Eu(III), hexadecyltrimethylammonium chloride (CTAC) (Sigma–Aldrich) and polyethyl glycol SH-PEG-NH_2 with molar masses of 200, 400, and 600 (Biochempeg Scientific Inc., USA) were employed (se Supporting Information for details).

Instrumentation: The photoirradiation of samples for controlled photosculpting, confocal luminescence microscopy, and collection of intensity time traces were performed using a Picoquant MicroTime 200 confocal microscope (Picoquant GmbH, Germany) based on an inverse microscope Olympus IX–71 (Olympus, Japan). For most experiments, the excitation source was a pulsed diode laser of 375 nm (LDH-375, Picoquant GmbH) working at controlled repetition frequency supplied by a Sepia II laser driver (Picoquant GmbH). Additional experiments (see Supporting Information for details) were performed using a 470 nm (LDH-470, Picoquant GmbH) or 635 nm (LDH-635, Picoquant GmbH) pulsed source. After the main dichroic mirror, a 405 LP longpass filter was used to eliminate the scattered laser light interference. The collected light was focused on a 75-µm pinhole and detected with a silicon avalanche photodiode (SPCM-AQR-14, PerkinElmer, USA) after passing through a 630/60 nm bandpass filter (Chroma Technology, USA). For comparison with the emission spectrum in Figure 1C, two silicon avalanche photodiodes were used with the abovementioned 630/60 bandpass filter and a 550/40 nm bandpass filter (Thorlabs, USA) and two hybrid photon multiplier tubes (Picoquant GmbH) with 450/40 and 500/40 nm bandpass filters (Thorlabs). For PLIM imaging, a train of pulses of 62.5 µs duration of the 375 nm laser (working at 80 MHz repetition rate) was used and a subsequent detection time window with the laser off of 5 ms, allowing for sufficient time to fully collect the PL emission decay of DTBTA-Eu(III). The pixel dwell time was 5.1 ms, although for PLIM imaging analysis, a 3 × 3 pixel spatial binning was performed to improve the reliability of the decay fitting. PLIM imaging was performed in SymphoTime 64 (Picoquant GmbH) using pixelwise tail fitting of the PL emission decay to a double-exponential decay function. The amplitudes associated with each decay time and the ratio of the amplitudes were analyzed using Fiji (distribution of ImageJ).[44]

Collection of the emission spectrum from the photosculpted Airy castles was performed by directing the collected light into an Andor Shamrock 303i-A spectrograph for spectral separation, and the light was detected with an ultrasensitive Andor Newton electron-multiplying CCD camera as described elsewhere.[45]

UV–visible absorption spectroscopy was carried out using a Lambda 650 spectrophotometer (PerkinElmer). Steady-state emission fluorimetry was performed with a Jasco FP-8300 (Jasco, Japan). Dynamic light scattering (DLS) measurements to obtain the NP size were performed using a Zetasizer µV (Malvern Panalytical, U.K.). TEM images were acquired on an FEI TECNAI T20 system (Tecnai, Eindhoven, The Netherlands) operated at 200 kV. TEM specimens were prepared by resuspension in deionized water, mild sonication for 30 s and subsequent deposition of 5 µL added onto a copper grid with a holey-type carbon layer (Electron Microscopy Sciences, Hatfield, PA, USA). Precision tweezers were used to hold the grid and allow the droplet to dry at room temperature in the absence of external light. SEM (FEG INSPECT-F50, FEI, Eindhoven, Netherlands) was used to acquire images and for EDX analysis. The equipment was operated at 10 kV using a 45° tilted configuration. Glass slides containing the Ag sculptures were sputtered with carbon using glow discharge (Leica Microsystems GmbH, Wetzlar, Germany EM ACE200 coater) to prevent sample charge events. AFM was performed using an NX20 microscope (Park Systems, South Korea) in noncontact mode with a cantilever ACTA operating at a resonant frequency of 269.89 kHz and a scan rate of 0.5 Hz at the core facilities at the University of Granada (Centro de Instrumentación Científica, CIC, Spain).

Photoirradiation of AgNRs and Photosculpting of Airy Castles: Photosculpting was carried out over glass slides (diameter = 25 mm) or into glass gridded slides (diameter = 28 mm) purchased from Ibidi GmbH, Germany. The slides were sequentially immersed in CTAB, Milli-Q water, and absolute ethanol, sonicating for 10 min in each step, and later immersed in 1 M HCl for 1 h. Then, the slides were immersed in 5% v/v (3-mercaptopropyl)trimethoxysilane in ethanol and washed with methanol; these steps were repeated three times. This process silanized the slides.

In a typical photosculpting experiment, 1 mL of an AgNR suspension was used to avoid evaporation effects during the process. The sample was irradiated at specific spots on the surface with the pulsed 375 nm laser for at least 60 s. After irradiation, Airy castles were controllably formed in the specific spots. The slide could be washed with water or ethanol without removing the Airy castles.

Photosculpting kinetics were analyzed by fitting the intensity time trace, $I(t)$, to an exponential rise function (Equation 1), where I_0 is the initial intensity, A is the amplitude, and k is the apparent growth rate.

$$I(t) = I_0 + A\left(1 - e^{-k \cdot t}\right) \quad (1)$$

Supporting Information

Supporting Information is available from the Wiley Online Library or from the author.

Acknowledgements

This work was supported by grant CTQ2017-85658-R funded by MCIN/AEI/10.13039/501100011033/FEDER "Una manera de hacer Europa", grant PID2020-114256RB-I00 funded by MCIN/AEI/10.13039/501100011033, and the diaRNAgnosis project funded by the European Union's Horizon 2020 research and innovation programme under the Marie Sklodowska-Curie grant agreement No 101007934. P.M.R.P. acknowledges funding from Fundação para a Ciência e a Tecnologia, I.P., through projects UIDB/00100/2020 and 2022.04076.PTDC. Funding for open access charge: Universidad de Granada / CBUA. The authors would like to acknowledge the Centro de Instrumentación Científica (CIC) of Universidad de Granada (Spain) and the Laboratorio de Microscopias Avanzadas, ICTS ELECMI (Spain) for the use of their AFM and TEM facilities.

Conflict of Interest

The authors declare no conflict of interest.

Data Availability Statement

The data that support the findings of this study are openly available in Digibug at http://dx.doi.org/10.30827/Digibug.81398, reference number 81398.

Keywords

metal-enhanced luminescence, microarrays, nanoclusters, nanorods, optical trapping, photodeposition

Received: January 18, 2023
Revised: April 8, 2023
Published online:

[1] C. J. Bustamante, Y. R. Chemla, S. Liu, M. D. Wang, *Nat. Rev. Methods Primers* **2021**, *1*, 25.
[2] C. Bradac, *Adv. Opt. Mater.* **2018**, *6*, 1800005.
[3] Y. Yang, Y. Ren, M. Chen, Y. Arita, C. Rosales-Guzmán, *Adv. Photonics* **2021**, *3*, 034001.
[4] M. L. Juan, M. Righini, R. Quidant, *Nat. Photonics* **2011**, *5*, 349.
[5] K. A. Forbes, D. S. Bradshaw, D. L. Andrews, *Nanophotonics* **2020**, *9*, 1.
[6] C.-H. Huang, T. Kudo, T. Sugiyama, H. Masuhara, J. Hofkens, R. Bresolí-Obach, *J. Phys. Chem. C* **2021**, *125*, 19013.
[7] Z. Yan, R. A. Shah, G. Chado, S. K. Gray, M. Pelton, N. F. Scherer, *ACS Nano* **2013**, *7*, 1790.
[8] C.-H. Huang, B. Louis, R. Bresolí-Obach, T. Kudo, R. Camacho, I. G. Scheblykin, T. Sugiyama, J. Hofkens, H. Masuhara, *Nat. Commun.* **2022**, *13*, 5325.
[9] T. Kudo, S.-F. Wang, K.-i. Yuyama, H. Masuhara, *Nano Lett.* **2016**, *16*, 3058.
[10] L. Bosanac, T. Aabo, P. M. Bendix, L. B. Oddershede, *Nano Lett.* **2008**, *8*, 1486.
[11] a) G. González-Rubio, A. Guerrero-Martínez, L. M. Liz-Marzán, *Acc. Chem. Res.* **2016**, *49*, 678; b) Y. A. Attia, M. T. Flores-Arias, D. Nieto, C. Vázquez-Vázquez, G. F. De La Fuente, M. A. López-Quintela, *J. Phys. Chem. C* **2015**, *119*, 13343; c) T. Tsuji, T. Yahata, M. Yasutomo, K. Igawa, M. Tsuji, Y. Ishikawa, N. Koshizaki, *Phys. Chem. Chem. Phys.* **2013**, *15*, 3099; d) D. Werner, A. Furube, T. Okamoto, S. Hashimoto, *J. Phys. Chem. C* **2011**, *115*, 8503; e) S. Link, C. Burda, B. Nikoobakht, M. A. El-Sayed, *J. Phys. Chem. B* **2000**, *104*, 6152.
[12] G. González-Rubio, P. Díaz-Núñez, A. Rivera, A. Prada, G. Tardajos, J. González-Izquierdo, L. Bañares, P. Llombart, L. G. Macdowell, M. Alcolea Palafox, L. M. Liz-Marzán, O. Peña-Rodríguez, A. Guerrero-Martínez, *Science* **2017**, *358*, 640.
[13] a) A. A. Unal, A. Stalmashonak, G. Seifert, H. Graener, *Phys. Rev. B* **2009**, *79*, 115411; b) A. V. Podlipensky, V. Grebenev, G. Seifert, H. Graener, *J. Luminesc.* **2004**, *109*, 135.
[14] A. Jakab, C. Rosman, Y. Khalavka, J. Becker, A. Trügler, U. Hohenester, C. Sönnichsen, *ACS Nano* **2011**, *5*, 6880.
[15] X. Zhuo, M. Henriksen-Lacey, D. Jimenez de Aberasturi, A. Sánchez-Iglesias, L. M. Liz-Marzán, *Chem. Mater.* **2020**, *32*, 5879.
[16] A. Delgado-Gonzalez, E. Garcia-Fernandez, T. Valero, M. V. Cano-Cortes, M. J. Ruedas-Rama, A. Unciti-Broceta, R. M. Sanchez-Martin, J. J. Diaz-Mochon, A. Orte, *ACS Omega* **2018**, *3*, 144.
[17] a) I. Díez, M. Pusa, S. Kulmala, H. Jiang, A. Walther, A. S. Goldmann, A. H. E. Müller, O. Ikkala, R. H. A. Ras, *Angew. Chem., Int. Ed.* **2009**, *48*, 2122; b) P. Sun, Z. Wang, Y. Bi, D. Sun, T. Zhao, F. Zhao, W. Wang, X. Xin, *ACS Appl. Nano Mater.* **2020**, *3*, 2038.
[18] C. Bu, L. Mu, X. Cao, M. Chen, G. She, W. Shi, *Nanotechnology* **2018**, *29*, 295501.
[19] F. Linares, E. García-Fernández, F. J. López-Garzón, M. Domingo-García, A. Orte, A. Rodríguez-Diéguez, M. A. Galindo, *Chem. Sci.* **2019**, *10*, 1126.
[20] M. Davies, A. Wochnik, F. Feil, C. Jung, C. Bräuchle, C. Scheu, J. Michaelis, *ACS Nano* **2012**, *6*, 6049.
[21] N. Nedyalkov, A. Dikovska, M. Koleva, N. Stankova, R. Nikov, E. Borisova, T. Genova, L. Aleksandrov, R. Iordanova, M. Terakawa, *Opt. Mater.* **2020**, *100*, 109618.
[22] F. A. Merchant, K. A. Bartels, A. C. Bovik, K. R. Diller, *Handbook of Image and Video Processing*, 2nd ed. (Ed: A. L. Bovik), Academic Press, Burlington **2005**, pp. 1291–1309.
[23] a) H. Kirshner, F. Aguet, D. Sage, M. Unser, *J. Microsc.* **2013**, *249*, 13; b) EPFL, http://bigwww.epfl.ch/algorithms/psfgenerator/, (accessed: January 2023).
[24] Y. Khalavka, C. Ohm, L. Sun, F. Banhart, C. Sönnichsen, *J. Phys. Chem. C* **2007**, *111*, 12886.
[25] T. Kudo, S.-J. Yang, H. Masuhara, *Nano Lett.* **2018**, *18*, 5846.
[26] C. Voisin, N. Del Fatti, D. Christofilos, F. Vallée, *J. Phys. Chem. B* **2001**, *105*, 2264.
[27] K. Yamada, K. Miyajima, F. Mafuné, *J. Phys. Chem. C* **2007**, *111*, 11246.
[28] T. Tsuji, Y. Higashi, M. Tsuji, Y. Ishikawa, N. Koshizaki, *Appl. Surf. Sci.* **2015**, *348*, 10.
[29] a) T. Baldacchini, A.-C. Pons, J. Pons, C. N. LaFratta, J. T. Fourkas, Y. Sun, M. J. Naughton, *Opt. Express* **2005**, *13*, 1275; b) Y.-Y. Cao, X.-Z. Dong, N. Takeyasu, T. Tanaka, Z.-S. Zhao, X.-M. Duan, S. Kawata, *Appl. Phys. A* **2009**, *96*, 453; c) N. Tsutsumi, K. Nagata, W. Sakai, *Appl. Phys. A* **2011**, *103*, 421.
[30] P. Ahonen, T. Laaksonen, A. Nykänen, J. Ruokolainen, K. Kontturi, *J. Phys. Chem. B* **2006**, *110*, 12954.
[31] A. K. Popov, J. Brummer, R. S. Tanke, G. Taft, M. Loth, R. Langlois, A. Wruck, R. Schmitz, *Laser Phys. Lett.* **2006**, *3*, 546.
[32] R. Pilot, M. Massari, *Chem. Phys. Impact* **2021**, *2*, 100014.
[33] A.-A. El Mel, R. Gautier, N. Stephant, P.-Y. Tessier, Y. Haik, *Nano-Struct. Nano-Objects* **2019**, *19*, 100320.
[34] H. Minamimoto, H. Irie, T. Uematsu, T. Tsuda, A. Imanishi, S. Seki, S. Kuwabata, *Chem. Lett.* **2015**, *44*, 312.
[35] B. Yang, N. Lu, D. Qi, R. Ma, Q. Wu, J. Hao, X. Liu, Y. Mu, V. Reboud, N. Kehagias, C. M. S. Torres, F. Y. C. Boey, X. Chen, L. Chi, *Small* **2010**, *6*, 1038.
[36] P. R. Ferreira, W. Correr, C. R. Mendonça, J. M. P. Almeida, *J. Nanopart. Res.* **2020**, *22*, 260.
[37] P. M. R. Paulo, P. Zijlstra, M. Orrit, E. Garcia-Fernandez, T. C. S. Pace, A. S. Viana, S. M. B. Costa, *Langmuir* **2017**, *33*, 6503.
[38] Y. Jeong, Y.-M. Kook, K. Lee, W.-G. Koh, *Biosens. Bioelectron.* **2018**, *111*, 102.
[39] T. Nishioka, J. Yuan, Y. Yamamoto, K. Sumitomo, Z. Wang, K. Hashino, C. Hosoya, K. Ikawa, G. Wang, K. Matsumoto, *Inorg. Chem.* **2006**, *45*, 4088.
[40] E. Garcia-Fernandez, S. Pernagallo, J. A. González-Vera, M. J. Ruedas-Rama, J. J. Díaz-Mochón, A. Orte, in *Fluorescence in Industry*, Vol. *18* (Ed: B. Pedras), Springer International Publishing, Cham **2019**, pp. 213–267.
[41] a) J.-F. Li, C.-Y. Li, R. F. Aroca, *Chem. Soc. Rev.* **2017**, *46*, 3962; b) D. Darvill, A. Centeno, F. Xie, *Phys. Chem. Chem. Phys.* **2013**, *15*, 15709.
[42] J. Patarroyo, A. Genç, J. Arbiol, N. G. Bastús, V. Puntes, *Chem. Commun.* **2016**, *52*, 10960.
[43] J. Schindelin, I. Arganda-Carreras, E. Frise, V. Kaynig, M. Longair, T. Pietzsch, S. Preibisch, C. Rueden, S. Saalfeld, B. Schmid, J.-Y. Tinevez, D. J. White, V. Hartenstein, K. Eliceiri, P. Tomancak, A. Cardona, *Nat. Methods* **2012**, *9*, 676.
[44] M. Kazem-Rostami, A. Orte, A. M. Ortuño, A. H. G. David, I. Roy, D. Miguel, A. Garci, C. M. Cruz, C. L. Stern, J. M. Cuerva, J. F. Stoddart, *J. Am. Chem. Soc.* **2022**, *144*, 9380.

